CMOS-Compatible Gas Sensors

L. Filipovic and S. Selberherr

Abstract— **As transistor scaling along Moore's law approaches its physical limits, the semiconductor industry has been intensely working on functional integration of devices along the More-than-Moore approach. The integration of sensors, RF circuits, and other functionalities with electronics is enabled by innovations in packaging, three-dimensional integration, and most importantly through the fabrication of multiple components and features on silicon using established technology. With the application of semiconductor metal oxide (SMO) thin films, there is potential for the integration of gas sensors with processing electronics. This manuscript describes SMO gas sensors, their fabrication, and operating techniques which require high temperatures and therefore an integrated microheater. Microheaters require the fabrication of a membrane in order to isolate the high temperature component from other circuitry. Finally, the manuscript looks at recent achievements in engineering of SMO films and in understanding and modeling their sensing mechanism.**

I. Introduction

Aggressive device scaling has been the driving force behind many advancements made in the microelectronics industry over the past several decades. As the miniaturization trend for complementary metal oxide semiconductor (CMOS) devices along the path of Moore's law [1], [2] continues, the typical transistor scaling is reaching its physical limits. This has caused the industry to look increasingly at different semiconductor materials and vertical transistor architectures, but also at the potential for the integration of multiple functionalities on a single chip or device, appropriately labeling this type of integration as Moore-than-Moore [3], [4]. The interest in the Internet of Things (IoT) and Internet of Everything (IoE) are clear indicators of this trend, where multi-featured electronics are packaged together. The first attempts at this multi-application packaging and integration was by electrically connecting different dies using bond wires. However, this approach is not ideal, since long bonding wires result in high resistance-capacitance (RC) delays, limiting the high frequency performance of the device and increasing the power dissipation. An increase in efficiency was recently achieved by applying three-dimensional (3D) integration using through silicon vias (TSVs).

With 3D integration, different dies are stacked on top of each other and their interconnections are managed using TSVs which provide an electrical contact between the front and back of a wafer. Using this approach, the RC delay and package size can be significantly reduced. Ultimately, achieving a full integration of all necessary components on a single wafer as a System-on-Chip (SoC) would be the optimal solution. Using silicon as a substrate for functionalities beyond integrated circuits and transistors, including radio frequency (RF) components, sensors and actuators, or biochips, would allow for an efficient integration between CMOS and micro-electro-mechanical systems (MEMS) devices into a monolithic device. From the fabrication side, the integration of added functionalities must be performed after the CMOS front end of line (FEOL) devices are in place, meaning that the same rules as those existing for back end of line (BEOL) metalization apply. With this in mind, a part of the challenge is that the temperature of all additional processing steps used to fabricate the added functionalities must be kept below 450°C so as to not damage the FEOL devices.

In the following sections we introduce currently existing gas sensing mechanisms while concentrating on the semiconducting metal oxide (SMO) gas sensor due to the recent achievements made in its integration with CMOS technology. The rest of the manuscript is divided into three sections: First, the processing techniques used to fabricate this gas sensor are described, including the membrane release and sensing layer deposition. Subsequently, we discuss the features of the sensors critical to operation and reliability, the microheater, and the SMO sensing layer. Finally, we discuss the sensor operation in terms of the current understanding of the sensing mechanism of SMO films.

A. Mechanisms for gas sensing

While the human nose can detect many different odors in our environment, it is unable to detect many harmful gases and it fails outright, when there is a need to detect a specific gas concentration. Even though many harmful gases are regularly present in our environment, it is not until a certain critical concentration is reached that they become harmful to our health and well-being. The ability to detect specific gas concentrations electrically is a research field which has been studied extensively over many decades. Many applications and industries rely on - or could greatly benefit from - the development of efficient and affordable gas sensors including health and safety [5], [6], automotive and aviation [7], [8], environmental monitoring [9], [10], [11], [12], and chemical warfare detection [13], [14], [15], just to name a few. More recently, the push in sensor research has been towards device integration in

L. Filipovic and S. Selberherr are with the Institute for Microelectronics, Technische Universität Wien, 1040 Vienna, Austria, E-mail: {filipovic|selberherr}@iue.tuwien.ac.at

978-1-7281-3418-5/19/$31.00 ©2019 IEEE

portable electronics such as smart-watches, smart-rings, smart-phones, tablets and wearables [16], [17]. Alongside portable electronics, fabrication and process controls, laboratory analytics, and smart-homes can be made more affordable, if cheaper gas sensing devices and equipment was available. Here, we examine current mechanisms for gas sensing while paying extra attention to properties which affect a sensor's portability such as low power, low cost, and a small footprint.

Today, there is a large variety of gas sensing principles which have shown value to industry and research including semiconductor, optical, thermal, infrared (IR), quarz microbalance, catalytic, dielectric, electrochemical, electrolyte, and conductivity based ones [18], [19], [20], [21]. Of all the currently known gas sensing mechanisms it is the semiconductor - or more accurately the semiconducting metal oxide - sensor which provides the biggest advantage towards integration and portability. While the catalytic pellistor also enjoys low power consumption, cost, and a relatively small footprint, it's selectivity is very poor, while its sensitivity is poorer and response time is longer than that of an SMO sensor. The piezo-electric sensor, on the other hand, has an excellent sensitivity, accuracy, and response time, but its power consumption is a limitation to portability. The same can be said for the photo-ionization and IR adsorption sensors. The electro-chemical sensor requires a large footprint, while the sensitivity of a thermal pellistor is not up to par with an SMO sensor. All in all, the SMO sensor provides the most advantages over alternatives, especially when it comes to its sensitivity, response time, and potential for miniaturization and portability through very low power consumption, very low fabrication costs, and a very small footprint. The primary concerns about the operation of SMO gas sensors is their lack of selectivity and difficulty in removing the chemisorbed gas molecules after a sensing event.

B. Semiconducting metal oxide gas sensor

The sensing mechanism of an SMO film is based on a changing electrical resistance due to charge accumulation on its surface in the presence of a target gas. The gas molecule interacts with the film's surface and through chemisorption either donates or captures an electron to or from the sensing film, respectively. This makes it clear why selectivity is an issue, as there is no direct way to know precisely which molecule caused the difference in resistance, only that the resistance has changed. The selectivity can be artificially introduced through the use of a sensor array, where multiple sensors with different properties are activated simultaneously [22], [23], [24], [25], [26], [27]. The different properties can be created by having each sensor operate at a different temperature or by introducing a different dopant to each sensor, which is optimized for a particular gas molecule. The collected data can subsequently be processed with a variety of methods such as neural networks [27] or machine learning [28] algorithms.

As alluded to in the previous paragraph, temperature plays an important role in the operation of SMO sensors. In fact, the sensing mechanism is activated only at elevated temperatures in the range between 250°C and 500°C. This provides enough energy to allow surface reactions to take place. The need for high temperature operation means that a microheater must be incorporated into the sensor structure, which in-turn must be isolated from the remaining circuitry. Not having proper thermal isolation would be a significant hindrance to the concept of integration. Therefore, the microheater is most commonly fabricated within a MEMS membrane, which hosts the microheater and provides a platform for the SMO film and sensing electrodes. A typical membrane stack is depicted in Fig. 1.

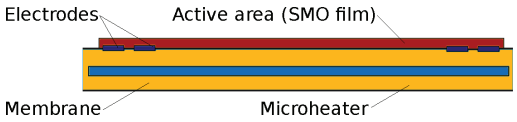

Fig. 1. SMO sensor membrane stack, depicting the "membrane" materials (SiO_2/Si_3N_4), the microheater, the electrodes, and the SMO sensing film, corresponding to the active area.

The formation of the aforementioned membrane is one of the most challenging steps in the fabrication of SMO sensors. There are two most commonly used MEMS membrane types: A closed or full membrane, where the active sensor area is isolated by removing the wafer underneath it and a suspended membrane, which is held in place by suspension beams above an air void. A perforated membrane, created using a sacrificial polyimide or using an additional photolithography step after a closed membrane is fabricated is an alternative option which has recently garnered some attention [29], [30]. In Fig. 1 we see that the membrane is composed of several layers, including the microheater, which could also have an additional heat spreading plate above it, the SMO film, electrodes, and the membrane stack. The membrane stack is composed of a combination of silicon dioxide (SiO_2) and silicon nitride (Si_3N_3) layers.

II. Sensor fabrication

Many fabrication steps are required for the SMO sensor. However, the two which present the most challenges are the membrane release, meaning the creation of a void under the membrane and the deposition of the SMO film. The main concern with the membrane release is that the fabrication should be compatible with CMOS technology to ensure easy integration with CMOS electronics, cost efficient fabrication, and low power consumption [31]. When depositing the sensing film itself, the ability to integrate this step within the CMOS sequence, or as a post-processing step, while ensuring a film of high quality, is of utmost importance.

A. Membrane release

The fabrication of the suspended membrane is one of the most critical steps in the creation of SMO gas sensors. As discussed in the previous section the types of membranes which can be fabricated are the closed, suspended, and perforated types. In Fig. 2a, Fig. 2b, and Fig. 2c, several recently published gas sensor designs which apply the closed membrane from [32], perforated membrane from [33], and suspended membrane from [34], respectively, are shown.

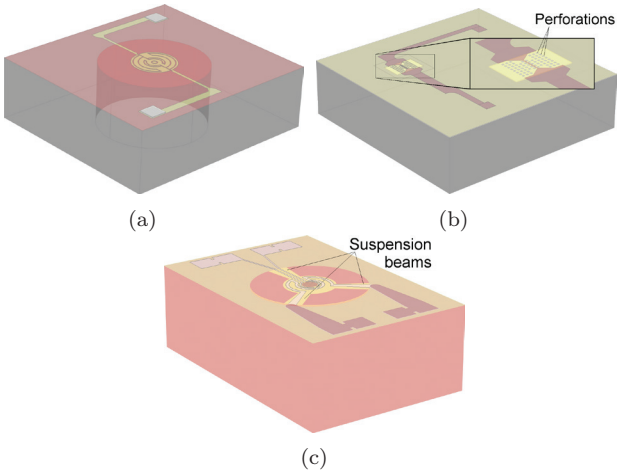

Fig. 2. Membrane types for gas sensors. (a) Closed membrane. (b) Perforated membrane. (c) Suspended membrane.

The steps required to fabricate the three membrane types shown in Fig. 2 are depicted in Fig. 3. The suspended membrane can be formed by patterning the suspension beams and front-side etching using an etchant with potassium hydroxide (KOH), tetra-methyl ammonium hydroxide (TMAH), ethylenediamine pyrocatechol (EDP), or by using selective plasma etching [35]. A primary goal is that the membranes are made very thin, resulting in a reduced power consumption. Furthermore, the fabrication technique utilizing patterning and etching is suitable for CMOS fabrication, since it is all performed from the front-side and no high temperature is required. However, wet etching is not a clean process and care must be taken to ensure that no other sections of the wafer are harmed during this step.

The closed membrane can be formed by etching from the back-side of the wafer using wet chemical etchants KOH, TMAH, and EDP or by the application of deep reactive ion etching (DRIE), which is a cyclical etching technique whereby each cycle consists of isotropic polymer deposition in fluorocarbon (e.g. C_4F_8) followed by one or more anisotropic etch steps, most frequently performed in ion-enhanced SF_6/O_2 plasma [36], [37]. It should be noted that the closed membrane can be turned into a perforated one by adding an extra front-side step where holes are patterned trough the membrane, as shown in Step 5. of Fig. 3c. The main advantage of the closed membrane is its mechanical stability. Because it is not suspended by thin beams, this structure can sustain higher thermal stresses, and therefore also higher operating temperatures. High stress in the beams can result in cracking and delamination, leading to a reduced device lifetime [38]. However, closed membranes generally dissipate more power, since more material is available to carry the heat away laterally.

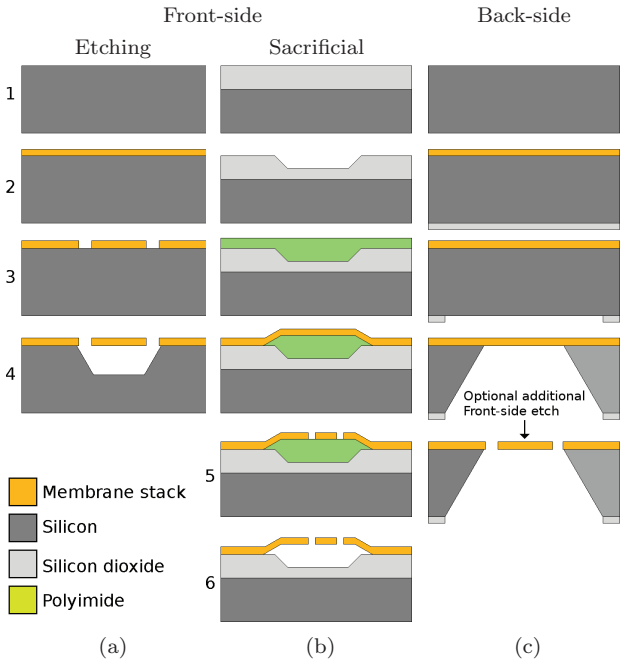

Fig. 3. Etching steps used to release the membrane for SMO gas sensors. (a) Front side etching for a suspended membrane. (b) Sacrificial Polyimide etching for a perforated membrane. (c) Back-side etching for a closed membrane.

The perforated membrane combines the benefits of the suspended and closed membranes. The structure is formed by introducing a sacrificial polyimide layer, depositing a membrane on top of it, then etching away the sacrificial layer using pre-patterned holes through the membrane. In addition to providing access to the sacrificial layer during etching, the holes help to reduce lateral heat conduction and heat losses through the membrane, thereby reducing the total power dissipation [29], [33]. For this structure, sacrificial polyimide HD8820 is deposited in a pre-etched SiO_2 cavity, then cured for one hour to obtain the desired thickness, shown in Fig. 3b [33]. The perforated membrane can also be formed by etching holes in a closed membrane, shown in Step 5 of the back-side process in Fig. 3c.

The membrane stack is usually composed of thin Si_3N_4 and SiO_2 layers. The typical values of the post-deposition stresses of SiO_2 and Si_3N_4 are about 1GPa tensile and about 300MPa compressive, respectively. Placing a Si_3N_4 layer between two SiO_2 layers can help reduce the membrane stress to a value below 100MPa, which is essential to ensure its mechanical stability [39].

B. Sensing film deposition

Ever since the gas sensing capabilities of metal oxide films were discovered, different techniques have been successfully attempted to deposit thin and thick films in a way conducive to integration with CMOS foundry technology. The sensing films can be deposited using physical or chemical methods. The chemical methods can be separated according to whether the chemical interaction with the surface takes place while the depositant is in the gas phase or in the liquid phase. One physical process which has been applied to deposit quality SMO films is sputtering [40], [41].

The chemical processes which have been examined for thin SMO film deposition are given in Fig. 4, where chemical vapor deposition (CVD) and atomic layer epitaxy (ALE) are the gas processes mentioned. Spray pyrolysis is shown as a liquid phase deposition technique. While it is true that spray pyrolysis starts from a liquid source which is sprayed onto the surface where it is to be deposited, the actual deposition mechanism is more analogous to CVD. It was recently shown that the coverage around corners and edges of 3D structures are highly uniform using spray pyrolysis and that the spray direction does not influence the surface coverage or film thickness [42]. The first application of spray pyrolysis was carried out by Chamberlin and Skarman [43] in 1966 for the growth of CdS thin films for solar cells. Since then, it has been used for many SMO films, including SnO_x, In_2O_3, indium-tin-oxide (ITO), PbO, ZnO, ZrO_2, yttria-stabilized zirconia (YSZ), and many others [44], for solar cells, batteries, optoelectronic devices, and gas sensors [42].

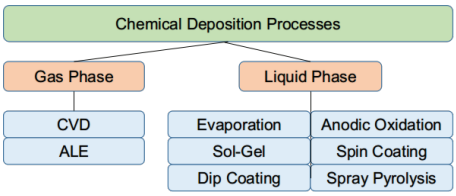

Fig. 4. Summary of chemical deposition techniques used for SMO film deposition.

The principal advantages of spray pyrolysis include:
- Integrable with CMOS technology since the deposition temperature is kept at about 400°C. While sputtering also allows this, it is a physical process which can result in non-uniform deposition and film thinning around corners and vertical walls, limiting the types of designs which can be used for the gas sensor.
- Cost effective. The necessary setup can be very straight-forwardly implemented as a post-CMOS processing step and does not require any cost-intensive equipment [45].
- Substrates with complex geometries can be coated and the resulting film has been shown to deposit very uniformly with a high quality for sensing [42], [45].

The main interest in spray pyrolysis stems from its cost effectiveness and possibility of integration in CMOS technology. The three steps which take place during spray pyrolysis deposition are summarized by:
1. Atomization of the precursor: The atomization is the act of applying pressure to push a liquid through a small nozzle, resulting in the formation of small droplets with an initial velocity, which compose the spray solution. The nozzle can be gas pressure based, ultrasonic, or electrostatic [46], while the resulting droplet size, rate of atomization, and droplet velocity are determined by the pressure applied and the nozzle diameter.
2. Aerosol transport of the droplet: The droplets travel through the air in liquid form towards their source due to several forces acting on them, finally reaching the surface. In the heated area, the droplets start to lose their volume, forming a precipitate, a vapor, or a powder, depending on the initial size of the droplet [42].
3. Decomposition of the precursor: This step initiates the film growth by interactions between the surface and the droplets which reach the surface in vapor form.

III. Sensor elements

The key elements of the SMO gas sensor are the sensing film itself and the microheater which, as mentioned previously, is necessary to heat the sensing film to an appropriately elevated temperature to initiate the sensing mechanism. The choices of materials used for the microheater and sensing film is critical to ensuring the proper selectivity towards a desired gas and high reliability. In this section we discuss the choice of materials and designs tested for the microheater and SMO sensing layer, recently attempted for gas sensor applications.

A. Microheater

Many materials have the potential to be used as a microheater, since the heating principle is based on Joule heating which is a phenomenon affecting many metals and semiconductors. Materials such as silicon carbide (SiC) [47], polysilicon [48], aluminum [49], copper [50], molybdenum [51], platinum [52], tungsten [32], nickel alloys [53], tantalum-aluminum (TaAl) [29], and many others have been used to heat the sensing film. There has been significant interest in SiC recently due to its high power density, potential for miniaturization, and low power consumption [54]. However, the use of SiC strays away from the typical silicon-based SiO_2/Si_3N_4 membrane stack, meaning its fabrication is more complex and not compatible with CMOS technology.

The initial materials used for microheater development were primarily those readily available in CMOS technology, such as polysilicon and aluminum [55]. However, these materials suffer from electromigration defects, when high current gradients are applied, and they have poor contact properties, a particular problem for high temperature operation. Today, platinum

is a popular choice due to its chemical inertness at high temperatures and its ability to deal with high current densities [40]. However, platinum is also not ideal because of its positive temperature coefficient of resistance (TCR), which magnifies hotpot effects, and its high cost. Hotspots can lead to potential drift in the response, which negatively affects the long-term reliability of the device [56]. Tungsten was recently suggested as a microheater material and it appears to be the perfect choice due to its resistance to electromigration; unfortunately, it has a tendency to form an oxide at temperatures above 300°C, so care must be taken when sealing the microheater in the membrane. Research into nickel and nickel alloys is currently ongoing due to several positive aspects of these thin films, including a low coefficient of thermal expansion (CTE), resistance to humidity, and a high Young's modulus. Tantalum-aluminum is another recently studied option [29] and its advantage is the ability to maintain its mechanical strength at elevated temperatures and its negative TCR. In summary, a good microheater material is one which has a low thermal conductivity, high electrical resistivity, high melting point, low CTE, low Poisson's ratio, and high compatibility with CMOS technology [40].

In addition to testing different materials for the microheater, innovative geometries and designs have been attempted in order to ensure a uniform temperature distribution across the active area and low power consumption. Some designs involve the placement of an additional highly thermally conductive plate below or above the microheater, which is electrically inert, in order to help distribute the heat more evenly [36]. While this is effective, it introduces an additional photolithography step, increasing fabrication costs. Some typical designs and patterns used for microheaters, in order to ensure good temperature uniformity, are shown in Fig. 5. The layout pitch (line and separation widths) has a significant influence on the efficiency of the temperature distribution [21]. Minimizing the separation leads to an improved power uniformity and reduced power dissipation. Having a predictable and uniform temperature is of primary importance to give confidence in the sensor's response, as can be extruded from Fig. 6. However, care should be taken to make sure novel designs do not introduce intricacies which increase the sensor's fabrication complexity, cost, and power consumption.

Recently, the influence of the microheater quality on the sensing behavior has been reported in [33]. The authors show that by introducing slight openings along the length of the microheater, with the goal of improving temperature uniformity, not only does the mechanical stability improve, but the sensitivity of the sensor does as well. The vertical displacement reduced from about 175nm to about 70nm when operating at 500°C, and the sensitivity of the sensor towards CH_2O and ethanol improved by 15% and 5%, respectively, without any increase in power dissipation which was about 10.5mW. Therefore, the microheater design must be treated as a core feature, influencing many aspects in the performance and reliability of a gas sensor.

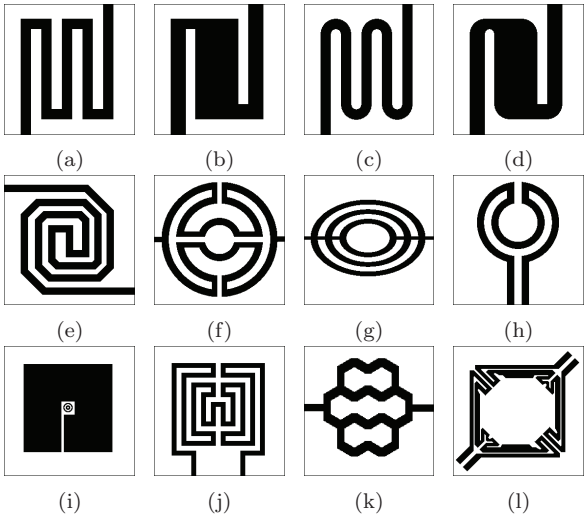

Fig. 5. Microheater geometries characterized and modeled over the last decades. These include the shapes: (a) Meander, (b) S-meander, (c) Curved, (d) S-curved, (e) Double spiral, (f) Drive wheel, (g) Elliptical, (h) Circular, (i) Plane plate, (j) Fin shape, (k) Honeycomb, and (l) Irregular.

B. Sensing film

The discovery of the sensing capabilities of SMO films has created a vision for the miniaturization, portability, and integration of gas sensors with CMOS electronics. In the 1950s Brattain and Bardeen [57] demonstrated that several semiconductor materials change their electrical resistivity when exposed to certain gas molecules, especially when heated to elevated temperature. The first device based on this effect was developed in the 1960s using a thin zinc oxide (ZnO) film [58], while by 1967 it was shown that adding small amounts of noble metal dopants, such as copper, platinum, rhodium, iridium, gold, or palladium can improve sensor performance [59].

Over the past decades, researchers have attempted to enhance gas sensor performance, including the sensitivity and selectivity of SMO films, by testing different SMO films and designing novel nanomaterials. Several SMO films which have been deposited using spray pyrolysis and used in various applications are given in Section II-B. For gas sensors in particular, ZnO, SnO_2, α-Fe_2O_3, CdO, $ZnSnO_4$, NiO, PbO, YSZ, WO_3, ITO, and In_2O_3, have been studied [60], [61]. From all the available materials tin oxide (SnO_2), an n-type wide band-gap semiconductor, has been investigated very frequently due to several excellent properties, including a high electron mobility of $160 cm^2 V^{-1} s^{-1}$ and high chemical and thermal stability [61]. Furthermore, SnO_2 has good sensitivity towards many gases and its deposi-

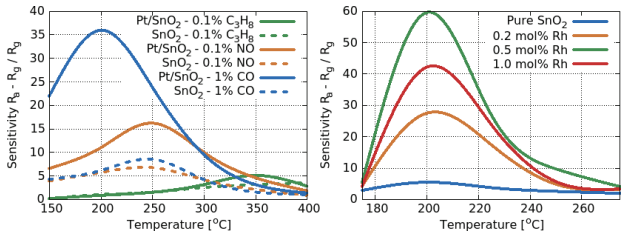

(a) (b)

Fig. 6. Sensitivity of doped and undoped SnO_2 sensors toward different gases as a function of operating temperature. (a) Pt-doped SnO_2 response to CO, NO, and C_3H_8 and (b) Rh-doped SnO_2 response to 50ppm acetone.

tion can easily and cost-effectively be incorporated into CMOS technology. For these reasons, SnO_2 shows the most promise for an integrated gas sensor and has recently been commercialized by several vendors [62], [63].

In Fig. 6 the sensitivities of several doped and undoped SnO_2 based sensors are summarized as a function of temperature. Fig. 6a shows that the addition of platinum results in an improved sensor signal response towards CO, NO, and C_3H_8, cf. [64], but a shift in the optimal operating temperature is also observed. Meanwhile, Fig. 6b shows that the presence of rhodium (Rh) can improve the sensing performance towards acetone, cf. [61], but that there is a peak amount of Rh doping which will improve performance. Of note is that 0.5 mol% Rh gives an improved sensitivity to 1.0 mol% Rh. A similar phenomenon was observed by Mädler et al. [65] regarding Pt impurities in SnO_2. The authors showed that, while a 0.2wt% Pt concentration improved the sensitivity, increasing this to 2wt% Pt reduced the sensing response significantly, even below pure SnO_2 levels. One part of the reason for the low signal is likely due to a "localized" consumption of gas molecules by Pt without electron transfer, resulting in no changes in the SnO_2 film's resistivity.

IV. Sensing mechanism

As of yet, a comprehensive and complete understanding of the sensing mechanism of SMO films is not available. However, significant progress has recently been made in understanding the conductivity and surface adsorption effects in SnO_2. Sensing is based on the concept of reception - of an analyte gas on an SMO layer through a surface chemical reaction - and transduction - changes at the SMO layer surface, which influence the conductive properties of the film [66]. The conduction inside the SnO_2 layer can be described using drift-diffusion equations [67], which are commonly used to model charge transport in semiconductors [68]. The thicknesses of the SMO layers used in gas sensors are comparable to the mean free path of the charge carriers, meaning that the diffusion component can be ignored. Using electrons as majority carriers, as is the case for the n-type semiconductor SnO_2, the conductivity σ is

$$\sigma = q \cdot n \cdot \mu_n, \tag{1}$$

where q is the electron charge, n is the electron concentration, and μ_n is the electron mobility. Both n and μ_n can vary significantly with temperature, meaning that both the surface reaction and conductivity of the sensing film are influenced by temperature [68].

A. Surface adsorption

The sensitivity of any film is primarily driven by its surface-to-volume ratio, since sensing is the effective change in a volume behavior due to surface reactions taking place. While many different structures are currently under investigation, the typical SMO sensor which is in production today is based on a porous film. The film is comprised of many grains which expose their external surface to the target gas, thereby increasing the effective surface-to-volume ratio. In addition to the drift in the grains, the conductivity involves electron transport through grain-grain, grain-bulk, and grain-electrode interfaces [69]. Since the charge mobility does not change during molecular adsorption, the sensing mechanism depends purely on increasing or decreasing charge concentrations [70]. Therefore, the sensing takes place through charge manipulation by gas molecules adsorbed on the surface of the film or grains and the resulting formation a charge depletion region [21].

The sensing of a target gas (e.g. CO) on SnO_2 starts by oxygen being ionosorbed on the SnO_2 surface, taking one (O^-) or two (O^{-2}) electrons from the SnO_2 bulk and creating a depletion region around the grain, as depicted in Fig. 7a. Then, in the presence of CO gas, CO molecules react with the surface oxygen, releasing the electron back, reducing the thickness of the depletion region and creating CO_2 gas as a byproduct, as depicted in Fig. 7b [69], [70].

The discussion above assumes that sensing of reducing gases (e.g. CO) would only be enabled in the presence of oxygen. However, recent studies have shown that even when oxygen is depleted, the SMO film continues to show a sensing response, while no oxidation byproduct (e.g. CO_2) is found [71]. A proposed explanation is that CO gas molecules can directly interact with the surface atoms, thereby donating an electron to SnO_2 and forming an accumulation region, depicted in Fig. 7c. The most involved model for the sensing mechanism is presented in recent works by the group of Barsan and Weimar in [7], [70], [72], [73].

B. Influence of metal additives

As mentioned previously, noble metal additives have shown to increase the sensitivity and selectivity of SMO sensors. Using operando spectroscopy in [70], the authors show that nanosized Pt clusters are formed on the

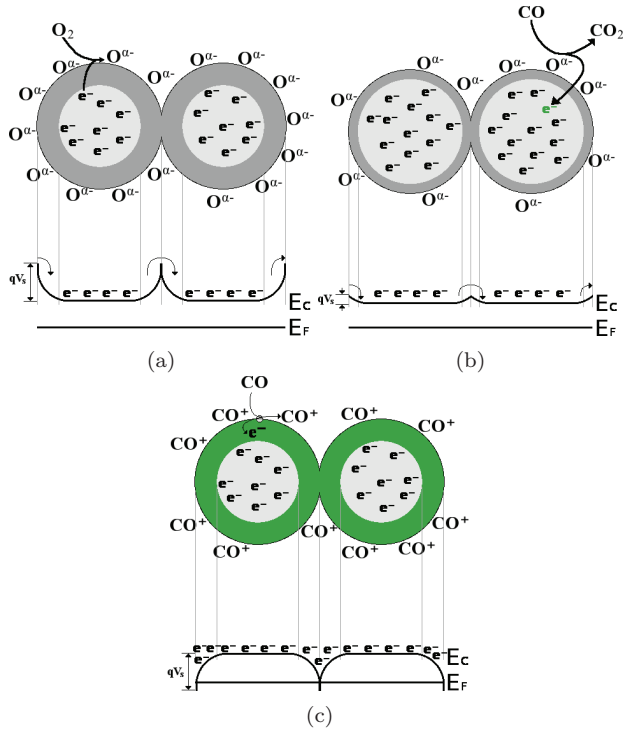

Fig. 7. Gas sensing and resulting band bending for a porous metal oxide, where the oxygen and reducing gas can penetrate to interact with grains. (a) Oxygen adsorbs on the surface, creating a depletion region, (b) CO reacts with oxygen, reducing the depletion region, and (c) after oxygen depletion, CO adsorbs on the surface, forming an accumulation region.

SnO_2 surface, acting as primary reaction sites for CO oxidation, thereby increasing the sensing effect. The amount of platinum determines whether CO oxidation or CO sensing will dominate, so simply adding more additive does not guarantee an improved response, which was discussed earlier and shown in Fig. 6b.

The ways in which a noble metal atom influences the sensing mechanism of an SMO film, including chemical and electrical sensitization, are described in some details in recent works, e.g. [7], [70], and a summary is given in Fig. 8. Chemical sensitization refers to the spill-over effect, which is attributed to metallic clusters which adsorb oxygen, and reducing gases, shown in Fig. 8a [74].

Electrical sensitization is based on the alignment of the Fermi levels of the SMO material and noble metal phase due to the different work function of the metal phase. The electrical contact between the two materials leads to a Fermi level alignment and therefore to surface band bending which is irrespective of the presence of any ionosorbed species, shown in Fig. 8b. Assuming no chemical or electrical interaction between the metal and the SMO film, the noble metal phase competes for adsorbed species with the SMO surface, decreasing the concentration of the target gas and hindering the sensing effect, as shown in the top of Fig. 8b [66]. However, in the case of an oxidation reaction taking place at the interface of the metal and the SMO film, an increased sensing behavior is also possible [7].

The metal atoms or ions are also able to incorporate themselves into the SnO_2 lattice, thereby changing the electrical and chemical characteristics of the film. In Fig. 8c the locations where the metal atom can incorporate into the SMO film and their effects are shown [66]. If the valence state of the metal ion is different from the replaced cation, new acceptor or donor states have the potential of being introduced [7]. In particular, doping with Pt leads to an increase in SnO_2 conductivity and an increased amount of oxygen vacancies acting as adsorption sites, thereby improving sensitivity.

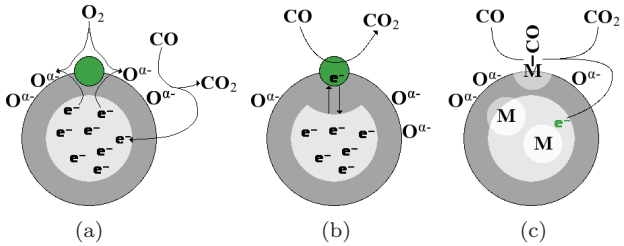

Fig. 8. Cross section of a grain within an SMO film, together with a noble metal doping. (a) The metal atom serves to spill over an oxygen molecule, slitting it into two atoms. (b) Fermi level control mechanism. (c) Possible donor/acceptor sites for the metal additive (M) are shown.

V. Conclusion

Significant progress has recently been achieved in the fabrication, design, and understanding of CMOS-compatible gas sensors based on semiconductor metal oxide films. These sensors are currently the most cost effective to fabricate, have excellent sensitivity towards many target gas species and environmental pollutants, operate at low power consumption, and their fabrication can be integrated in a mature CMOS foundry technology. The gas sensing mechanism involves the heating of a sensing film to several hundred degrees Celsius to activate the surface chemical reactions. The high temperature is provided using a microheater fabricated within a closed, suspended, or perforated membrane composed of several SiO_2 and Si_3N_4 layers.

In this manuscript we describe the fabrication process necessary to generate the three types of membranes as well as the deposition step used to introduce the SMO sensing film on top of this membrane stack. Furthermore, we summarize recent research to find the ideal microheater material and describe the geometrical designs which are meant to provide a uniform temperature distribution to the sensor. Finally, the sensing mechanism is discussed and recent achievements in understanding and modeling the surface reactions taking place during operation are described. The influence of noble metal additives on the sensing mechanism is also described.

References

[1] G. E. Moore, *Electronics*, vol. 38, no. 8, 1965.
[2] M. M. Waldrop, *Nature News*, vol. 530, no. 7589, pp. 144–147, 2016.
[3] W. Arden *et al.*, "More-than-Moore white paper," 2010.
[4] G. Q. Zhang and A. van Roosmalen, Eds., *More than Moore: Creating High Value Micro/Nanoelectronics Systems*. Springer Science & Business Media, 2010.
[5] H. Li *et al.*, *IEEE Sensors Journal*, vol. 14, no. 10, pp. 3391–3399, 2014.
[6] R. A. Potyrailo, *Chemical Reviews*, vol. 116, no. 19, pp. 11 877–11 923, 2016.
[7] S. A. Müller *et al.*, *ChemCatChem*, vol. 10, no. 5, pp. 864–880, 2018.
[8] R. Moos *et al.*, *Sensors and Actuators B: Chemical*, vol. 83, no. 1-3, pp. 181–189, 2002.
[9] G. Martinelli *et al.*, *Sensors and Actuators B: Chemical*, vol. 55, no. 2-3, pp. 99–110, 1999.
[10] M. C. Carotta *et al.*, *Sensors and Actuators B: Chemical*, vol. 58, no. 1-3, pp. 310–317, 1999.
[11] G. F. Fine *et al.*, *Sensors*, vol. 10, no. 6, pp. 5469–5502, 2010.
[12] G. Wysocki *et al.*, *Applied Optics*, vol. 46, no. 33, pp. 8202–8210, 2007.
[13] A. A. Tomchenko, G. P. Harmer, and B. T. Marquis, *Sensors and Actuators B: Chemical*, vol. 108, no. 1-2, pp. 41–55, 2005.
[14] F. Wang, H. Gu, and T. M. Swager, *Journal of the American Chemical Society*, vol. 130, no. 16, pp. 5392–5393, 2008.
[15] R. Yoo *et al.*, *Sensors and Actuators B: Chemical*, vol. 221, pp. 217–223, 2015.
[16] G. Neri, *Chemosensors*, vol. 3, no. 1, pp. 1–20, 2015.
[17] E. Singh, M. Meyyappan, and H. S. Nalwa, *ACS Applied Materials & Interfaces*, vol. 9, no. 40, pp. 34 544–34 586, 2017.
[18] G. Korotcenkov, *Materials Science and Engineering: B*, vol. 139, no. 1, pp. 1–23, 2007.
[19] G. Eranna *et al.*, *Critical Reviews in Solid State and Materials Sciences*, vol. 29, no. 3-4, pp. 111–188, 2004.
[20] A. Dey, *Materials Science and Engineering: B*, vol. 229, pp. 206–217, 2018.
[21] L. Filipovic and A. Lahlalia, *Journal of The Electrochemical Society*, vol. 165, no. 16, pp. B862–B879, 2018.
[22] B. T. Marquis and J. F. Vetelino, *Sensors and Actuators B: Chemical*, vol. 77, no. 1-2, pp. 100–110, 2001.
[23] N. Barsan, D. Koziej, and U. Weimar, *Sensors and Actuators B: Chemical*, vol. 121, no. 1, pp. 18–35, 2007.
[24] K. T. Ng, F. Boussaid, and A. Bermak, *IEEE Transactions on Circuits and Systems I: Regular Papers*, vol. 58, no. 7, pp. 1569–1580, 2011.
[25] T. Konduru, G. C. Rains, and C. Li, *Sensors*, vol. 15, no. 1, pp. 1252–1273, 2015.
[26] L. A. Horsfall *et al.*, *Journal of Materials Chemistry A*, vol. 5, no. 5, pp. 2172–2179, 2017.
[27] D. Zhang *et al.*, *Sensors and Actuators B: Chemical*, vol. 240, pp. 55–65, 2017.
[28] Y.-H. Liao *et al.*, *Sensors*, vol. 19, no. 8, p. 1866(15), 2019.
[29] A. Lahlalia *et al.*, *Journal of Microelectromechanical Systems*, vol. 27, no. 3, pp. 529–537, 2018.
[30] O. Le Neel *et al.*, "Miniature gas analyzer," Patent US 20 180 017 513 A1, January, 2018.
[31] E. Lackner *et al.*, *Materials Today: Proceedings*, vol. 4, no. 7, pp. 7128–7131, 2017.
[32] S. Z. Ali *et al.*, *IEEE Sensors Journal*, vol. 15, no. 12, pp. 6775–6782, 2015.
[33] A. Lahlalia *et al.*, *Sensors*, vol. 19, no. 2, p. 374(14), 2019.
[34] A. Lahlalia, L. Filipovic, and S. Selberherr, *IEEE Sensors Journal*, vol. 18, no. 5, pp. 1960–1970, 2018.
[35] C. Dücsö *et al.*, *Sensors and Actuators A: Physical*, vol. 60, no. 1-3, pp. 235–239, 1997.
[36] R. Coppeta *et al.*, in *Sensor Systems Simulations*, W. D. van Driel, O. Pyper, and C. Schumann, Eds. Springer Nature Switzerland AG, 2020; Chapter 2, pp. 17–72.
[37] F. Lärmer and A. Urban, *Microelectronic Engineering*, vol. 67, pp. 349–355, 2003.
[38] A. I. Uddin, D.-T. Phan, and G.-S. Chung, *Sensors and Actuators B: Chemical*, vol. 207, pp. 362–369, 2015.
[39] L. Filipovic and S. Selberherr, *IEEE Transactions on Device and Materials Reliability*, vol. 16, no. 4, pp. 483–495, 2016.
[40] I. Simon *et al.*, *Sensors and Actuators B: Chemical*, vol. 73, no. 1, pp. 1–26, 2001.
[41] M. Frietsch *et al.*, *Sensors and Actuators B: Chemical*, vol. 65, no. 1-3, pp. 379–381, 2000.
[42] L. Filipovic *et al.*, *IEEE Transactions on Semiconductor Manufacturing*, vol. 27, no. 2, pp. 269–277, 2014.
[43] R. Chamberlin and J. Skarman, *Journal of the Electrochemical Society*, vol. 113, no. 1, pp. 86–89, 1966.
[44] J. B. Mooney and S. B. Radding, *Annual Review of Materials Science*, vol. 12, no. 1, pp. 81–101, 1982.
[45] E. Brunet *et al.*, *Sensors and Actuators B: Chemical*, vol. 165, no. 1, pp. 110–118, 2012.
[46] D. Perednis, "Thin film deposition by spray pyrolysis and the application insolid oxide fuel cells," Ph.D. dissertation, ETH Zürich, 2003.
[47] F. Solzbacher *et al.*, *Sensors and Actuators B: Chemical*, vol. 64, no. 1-3, pp. 95–101, 2000.
[48] S. Astié *et al.*, *Sensors and Actuators B: Chemical*, vol. 67, no. 1-2, pp. 84–88, 2000.
[49] N. Abedinov *et al.*, *Journal of Vacuum Science & Technology A: Vacuum, Surfaces, and Films*, vol. 19, no. 6, pp. 2884–2888, 2001.
[50] Y. S. Kim, *Sensors and Actuators B: Chemical*, vol. 114, no. 1, pp. 410–417, 2006.
[51] L. L. R. Rao *et al.*, *IEEE Sensors Journal*, vol. 17, no. 1, pp. 22–29, 2016.
[52] F. Mailly *et al.*, *Sensors and Actuators A: Physical*, vol. 94, no. 1-2, pp. 32–38, 2001.
[53] S. Roy, C. Sarkar, and P. Bhattacharyya, *Solid-State Electronics*, vol. 76, pp. 84–90, 2012.
[54] F. Solzbacher *et al.*, *Sensors and Actuators B: Chemical*, vol. 77, no. 1-2, pp. 111–115, 2001.
[55] K. Zhang, S. Chou, and S. Ang, *International Journal of Thermal Sciences*, vol. 46, no. 6, pp. 580–588, 2007.
[56] L. Xu *et al.*, *IEEE Sensors Journal*, vol. 11, no. 4, pp. 913–919, 2010.
[57] W. H. Brattain and J. Bardeen, *The Bell System Technical Journal*, vol. 32, no. 1, pp. 1–41, 1953.
[58] T. Seiyama *et al.*, *Analytical Chemistry*, vol. 34, no. 11, pp. 1502–1503, 1962.
[59] P. Shaver, *Applied Physics Letters*, vol. 11, no. 8, pp. 255–257, 1967.
[60] L. Filipovic and S. Selberherr, *Sensors*, vol. 15, no. 4, pp. 7206–7227, 2015.
[61] X. Kou *et al.*, *Sensors and Actuators B: Chemical*, vol. 256, pp. 861–869, 2018.
[62] Figaro USA, Inc., "TGS 8100."
[63] SGX SENSORTECH, "MiCS-6814 - MOS triple sensor."
[64] M. Saberi, Y. Mortazavi, and A. Khodadadi, *Sensors and Actuators B: Chemical*, vol. 206, pp. 617–623, 2015.
[65] L. Mädler *et al.*, *Journal of Nanoparticle Research*, vol. 8, no. 6, pp. 783–796, 2006.
[66] D. Degler, "Spectroscopic insights in the gas detection mechanism of tin dioxide based gas sensors," Ph.D. dissertation, Eberhard Karls Universität Tübingen, 2017.
[67] G. Tulzer *et al.*, *Nanotechnology*, vol. 24, no. 31, p. 315501(10), 2013.
[68] L. A. Caffarelli and A. Vasseur, *Annals of Mathematics*, vol. 171, pp. 1903–1930, 2010.
[69] N. Barsan and U. Weimar, *Journal of Electroceramics*, vol. 7, no. 3, pp. 143–167, 2001.
[70] D. Degler *et al.*, *Journal of Materials Chemistry A*, vol. 6, no. 5, pp. 2034–2046, 2018.
[71] N. Bârsan, M. Hübner, and U. Weimar, *Sensors and Actuators B: Chemical*, vol. 157, no. 2, pp. 510–517, 2011.
[72] N. Barsan, J. Rebholz, and U. Weimar, *Sensors and Actuators B: Chemical*, vol. 207, pp. 455–459, 2015.
[73] D. Degler *et al.*, *The Journal of Physical Chemistry C*, vol. 119, no. 21, pp. 11 792–11 799, 2015.
[74] G. N. Vayssilov *et al.*, *The Journal of Physical Chemistry C*, vol. 115, no. 47, pp. 23 435–23 454, 2011.